ELSEVIER

Optics Communications 145 (1998) 57–63

OPTICS COMMUNICATIONS

Diffraction by cold atoms

F. Strauch, V. Gomer [1], H. Schadwinkel, B. Ueberholz, D. Haubrich, D. Meschede

Institut für Angewandte Physik, Universität Bonn, Wegelerstrasse 8, D-53115 Bonn, Germany

Received 1 May 1997; accepted 12 August 1997

Abstract

We have observed diffraction of a laser probe beam by a trapped sample of cold atoms. The effect is only visible in the vicinity of a resonance line. The observed diffraction pattern arises from interference of the incident and scattered light wave, allowing reconstruction of geometric properties of the trapped sample from the holographic record. © 1998 Elsevier Science B.V.

1. Introduction

Magnetooptical traps (MOTs) provide dense samples of atoms at very low velocities [1]. It is known that for frequencies near the atomic resonant transition such samples are optically thick with only 10^7 atoms at a density of 10^{10} cm^{-3} giving rise to strong absorption of a weak probe beam [2,3]. At an optical density close to unity also the trapping laser light is strongly absorbed and rescattered, causing a repulsive force and balancing the total number of atoms that may be accumulated [4].

In the vicinity of an atomic resonance line the wavefront of a probe beam illuminating a trapped sample of cold atoms not only experiences attenuation due to absorption but also strong phase shifts due to dispersion. We consider an isolated linear oscillator resonance for a simplified model only. At low atomic densities $n_{\mathrm{At}} < \lambda^{-3}$ the complex index of refraction n in the trapped sample is related to the atomic damping rate γ and the detuning δ of laser frequency from atomic resonance by

$$n = n' + in'' = 1 + \frac{3n_{\mathrm{At}}\lambda^3}{8\pi^2}\,\frac{i - 2\delta/\gamma}{1 + (2\delta/\gamma)^2}\,. \qquad (1)$$

For typical atomic densities $n_{\mathrm{At}} \simeq 10^{10}\,\mathrm{cm}^{-3}$ obtained in a MOT and a probe laser detuning δ of half a natural linewidth γ one estimates $|n' - 1| \simeq 10^{-4}$ for the real part of the refractive index. For a given sample the largest excess phase shift in comparison to vacuum is accumulated at $2\delta/\gamma = \pm 1$. When the sample of effective length D reaches an optical density of unity, $2kn''D = 1$, a significant maximum phase shift $|\Phi_0| = kD|n' - 1| = 1/2$, or an equivalent optical path difference of $\lambda/4\pi$ is calculated, even though the refractive index differs very little from unity. In high density storage devices, however, this phase shift is obviously much more prominent and may easily exceed 2π. Consequently dispersion may cause a notable backaction of the trapped atoms on the light beam, and also affects the trapping beams themselves. The influence on the wavefronts in the trapping region is of relevance for instance in the formation of optical lattices which are particularly interesting at high atomic densities [5] and hence strong dispersion.

We have observed diffraction of a probe laser beam from a cesium MOT (Fig. 1). Due to dispersion near an atomic resonance retardation or advancement of the scattered wave relative to the transmitted wave are expected. In very close analogy to in-line holography [6] the diffraction pattern observed is caused by the interference of the incident reference wave and the scattered object wave. A similar method is in fact used in optical instruments sizing particles in a three-dimensional volume. There were also experiments that observed the diffraction from an atomic beam [7]. Experiments exploring the case of very high densities have recently been performed in connection with atomic Bose-Einstein condensates [8]. It is the purpose of

[1] Corresponding author. E-mail: gomer@iap.uni-bonn.de.

PII S0030-4018(97)00470-7

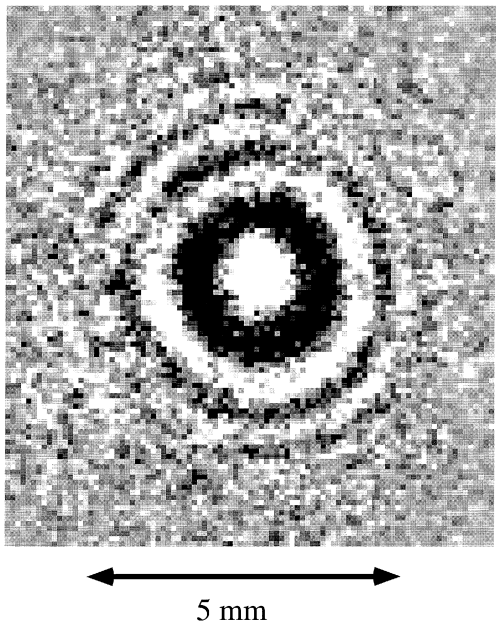

Fig. 1. 2D intensity distribution of the diffraction pattern on a screen at 1.88 m separation from the MOT. The background intensity is subtracted. Probe laser detuning is -4 MHz from the unshifted $F = 4 \rightarrow F' = 5$ line center.

this work to investigate the dispersive aspect of light interaction with a magnetooptically trapped sample of atoms at moderate densities and to discuss the information content of the diffraction pattern with regard to the total number of trapped atoms, and the spatial density distribution.

2. Experimental

We use a standard MOT which captures cesium atoms from the background gas. The trapping laser fields detuned to the red from the D_2 line (wavelength $\lambda = 852.1$ nm) are derived from a commercial Ti:sapphire laser locked to a reference cavity. A beat note with a diode laser stabilized to the center of the cesium cooling transition $F = 4 \rightarrow F' = 5$ (master laser) is observed to monitor the detuning. Repumping is provided by an additional diode laser. Details of our apparatus have been published elsewhere [9].

A probe laser beam illuminating the trapped atom sample propagates in the plane perpendicular to the MOT symmetry axis and crosses the two other cooling laser beams at an angle of 45°. The probe beam is spatially filtered with an optical single mode fiber to obtain a smooth Gaussian profile. The $1/e^2$ diameter of the probe beam (13.1 mm) is much larger than the MOT size (typically 0.3 mm). The intensity of the probe beam was kept well below the saturation intensity of 1.1 mW/cm^2 in order to minimize the influence on the dynamics of the trapped atoms. For quantitative analysis of the diffraction data with respect to trap size and density the probe laser detuning has to be precisely known. This is achieved by rf phase locking the probe laser to the master laser.

For a near resonant probe beam diffraction fringes (Fig. 1) are observed with a CCD camera on a screen 1.88 m separated from the MOT without any additional imaging. They resemble the diffraction patterns caused by a circular aperture. Diffraction causes a maximum 10% modulation of the total intensity in our experiment.

Very similar diffraction patterns are observed for all three hyperfine transitions to the $6^2P_{3/2}(F' = 3,4,5)$ levels of the cesium D_2 line starting from the $6^2S_{1/2}(F = 4)$ ground level. To the red side of every resonance line a bright center of the diffraction pattern is observed, to the blue side the center is dark, setting a notable contrast to conventional Fraunhofer diffraction by a pure amplitude object where a central maximum is always observed.

3. Theory

In the case of refractive indices near unity the light rays experience little bending by passing the scattering volume. Hence, in order to calculate the diffraction pattern it is sufficient to account for phase shifts only by integrating them along unbent rays by neglecting refraction. The extended (3D) scattering object is then effectively reduced to its two-dimensional 'projection' onto a plane perpendicular to the ray direction (all weak lenses are thin!).

According to scalar diffraction theory the wave E_P generated by the scattering object in an aperture area $\mathscr{A}$ is given by

$$E_P(r) = -\frac{i}{\lambda}\int\int_{\mathscr{A}} dx'\,dy'\,\frac{e^{iks}}{s}\,E(x',y',0), \qquad (2)$$

where s denotes the distance between the observation point $r = (x,y,z)$ and an arbitrary point $(x',y',0)$ in the scattering plane $\mathscr{A}$ at $z = 0$. The transverse amplitude distribution of the transmitted wave in a plane $\mathscr{A}$ immediately after the scattering object may be written as

$$E(x',y',0) = E_i(x',y',0)\,e^{i\Phi(x',y')}. \qquad (3)$$

Here $E_i(x,y,z) = E_0 G(x,y,z)$ describes the incident laser wave in the form of a fundamental Gaussian beam. The function $\Phi(x',y') = \int_{-\infty}^{+\infty} k[n(r') - 1]\,dz'$ in Eq. (3) gives the phase shift for a ray passing through the scattering object at (x',y') and it is proportional to the area density of the scattering cold atoms. Note that the phase shift Φ is complex and thus absorption is accounted for properly. The complex index of refraction $n(r')$ reflects the spatial distribution of atoms in the scattering sample and is of primary interest for us. Introduction of the form factor $F(x',y') = \exp[i\Phi(x',y')] - 1$ allows us to represent the transmitted wave as the sum of an undistorted incident

wave and a secondary wave E_s generated by the diffracting object

$$E_P(r) = E_0 G(x,y,z) - \frac{iE_0}{\lambda}\int\int_{\mathscr{A}} dx'\,dy'\,G(x',y',0)\,\frac{e^{iks}}{s}F(x',y') = E_i(r) + E_s(r). \quad (4)$$

For z large compared to the size of the scattering object D we conventionally replace $1/s$ in Eq. (4) by $1/z$ and expand s in the exponential function to $s \approx z + \rho^2/2z + \rho'^2/2z - \boldsymbol{\rho}\cdot\boldsymbol{\rho}'/z$. For a cylindrically symmetric problem the form factor is a function of ρ' only and hence the ϕ'-integration in Eq. (4) can be carried out. For a trap size much smaller than the probe beam diameter one can neglect the probe beam curvature in the scattering volume and set $G = 1$ in the integral (4). Furthermore, at sufficiently small densities $|\Phi_0| \approx |kD(n_0 - 1)| \ll 1$ we can expand the form factor to $F(x',y') \approx i\Phi(x',y')$ and find for the scattered wave

$$E_s(\rho,z) = \frac{E_0 k}{z}\,e^{ikz}\,e^{ik\rho^2/2z} \times \int_0^\infty d\rho'\,\rho'\,e^{ik\rho'^2/2z}\,J_0\left(\frac{k\rho\rho'}{z}\right)\Phi(\rho'), \quad (5)$$

where J_0 is the zero order Bessel function of the first kind and n_0 is the maximum index of refraction in the trap center. For the special case of a spherical Gaussian distribution the ρ'-integration in Eq. (5) can also be carried out explicitly. In our homogeneous model we neglect the influence of optical lattices which are known to be present in a MOT [5,10,11], and which could cause modifications since the scattering density can be concentrated with periodicities of commensurable length with the scattering wavelength. We then expect a Gaussian distribution function for a well adjusted MOT, which yields $\Phi(x',y') = \Phi_0 \exp(-\rho'^2/\omega_0^2)$ with the effective trap size $D = \sqrt{\pi}\,\omega_0$. The maximum complex phase shift for the central ray $\Phi_0 = \sqrt{\pi}\,k\omega_0(n_0 - 1)$ is determined by the extension ω_0 of the cloud and the index of refraction n_0.

The integration of Eq. (5) yields [12]

$$E_s(\rho,z) = E_0 i\Phi_0 \frac{\omega_0}{W}\exp\left[ikz - i\phi - \rho^2\left(\frac{1}{W^2} - \frac{ik}{2R}\right)\right]. \quad (6)$$

For the Gaussian density distribution the result is a cylindrical Gaussian TEM_{00}-mode with waist located at $z = 0$ and with usual notations for the Gaussian width $W(z) = \omega_0 \times \sqrt{1 + (z/z_0)^2}$, for the radius of wavefront curvature $R(z) = (z^2 + z_0^2)/z$, Rayleigh range $z_0 = k\omega_0^2/2$, and Gouy phase $\phi = \tan^{-1}(z/z_0)$.

Physically, this result is very transparent. Indeed, in this limit ($|\Phi| \ll 1$) we can expand the amplitude distribution (3) in the plane $\mathscr{A}$ to

$$E(x',y',0) \approx E_i(x',y',0) + iE_i(x',y',0)\Phi(x',y'), \quad (7)$$

which yields $E_s(x',y',0) = iE_i(x',y',0)\Phi_0 \exp(-\rho'^2/\omega_0^2)$. Hence the scattered wave directly after the scattering object has a Gaussian field distribution. The propagation of Gaussian waves with z is known. Therefore one can directly construct the expected diffraction pattern at separation z from the scattering sample from Eq. (4) as the sum of an undistorted incident wave and the Gaussian

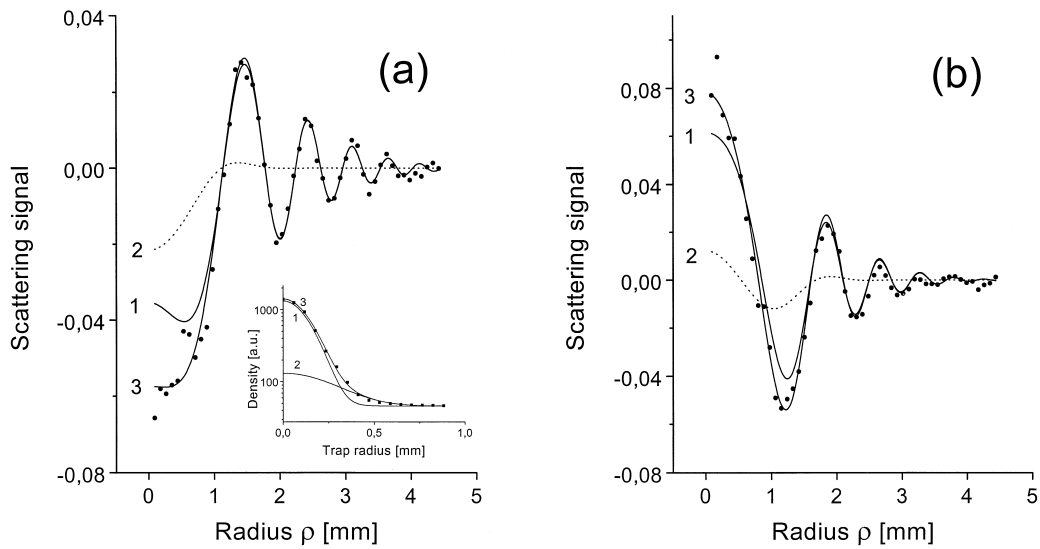

Fig. 2. Radial dependence of the diffraction pattern intensity (dots), averaged over the azimuthal angle for probe laser detuning of $+25$ MHz (a) and -4 MHz (b). The lines are fits to the data assuming one Gaussian beam (1), the residual (2, dashed) and two Gaussian beams (3). The inset shows the fluorescence intensity distribution of the trap (squares) with two Gaussian components 1 and 2.

beam generated by the diffracting object without explicit calculation of the Kirchhoff integral (2).

In the first order of Φ_0 the diffraction pattern normalized by the undistorted incident wave is now given by

$$\frac{|E_i + E_s|^2 - |E_i|^2}{E_0^2 G(\rho, z)} = -2|\Phi_0|\frac{\omega_0}{W}\cos\left[\arg\Phi_0 - \phi + \frac{k\rho^2}{2}\left(\frac{1}{R} - \frac{1}{R_p}\right)\right]\exp(-\rho^2/W^2), \tag{8}$$

where $i\Phi_0 \equiv -|\Phi_0|\exp(i\arg\Phi_0)$ and R_p describes the probe beam curvature radius at the observation screen.

4. Results

In a first series of experiments we recorded diffraction patterns under constant trapping conditions (trapping laser intensity of 4.5 mW/cm^2 per beam, detuning equal to one natural line width) for different probe laser detunings. For background elimination the probe laser beam profile is subtracted from the diffraction picture. A radial cross section of the two-dimensional camera picture is obtained by averaging on concentric circles. Two examples of radial diffraction profiles for blue and red probe laser detunings near the $F = 4 \rightarrow F' = 5$ transition are shown in Fig. 2. The fit (curve 1) according to Eq. (8) describes well the oscillatory part of the diffraction profiles. From this the curvature radius $R_p = 14.5$ m of the probe laser beam and and the trap waist $\omega_0 = 0.29$ mm are calculated. R_p agrees well with the probe beam curvature radius measured independently.

At small radii, however, the theoretical curve deviates significantly from the experimental result. Although our approximation $|\Phi_0| \ll 1$ is not rigorously justified (in our case $|\Phi_0| \approx 0.3$), an account for higher orders in scattering could not explain this deviation. Indeed, for high densities one can Taylor expand the form factor and obtain for the scattered wave a set of cylindrical Gaussian TEM$_{00}$-modes with widths $\omega_n^2 = \omega_0^2/n$. Thus, higher orders result in more divergent scattered waves with wider envelopes and cannot add a desirable correction (like the curves 2 in Fig. 2) to the diffraction pattern in the far field.

An explanation for the disagreement can be found in the deviations of the MOT profile from the Gaussian shape. From a camera picture of the trap we have learned that the density distribution of atoms can be well approximated by a superposition of two Gaussians with a ratio of widths and heights of 1:2 and 14.9:1 (see the inset in Fig. 2). The linear approximation allows us to construct the scattered waves from every cloud component independently. In the far field only the narrow component contributes significantly to the oscillatory wings (large ρ) of the diffraction pattern. Despite the relatively small density of the second wider component its contribution to the central part may be large (see curve 2 in Fig. 2) because the contribution is proportional to the total atom number in the corresponding component. Thus the envelope of the interference pattern on the screen is the sum of two Gaussian envelopes with relative amplitudes of approximately 2:1. With this correction the fit (curve 3) shows good agreement with the data.

In Fig. 3 we show the spectral behaviour of the scattering phase $\arg\Phi_0 - \phi$ and the amplitude $2|\Phi_0|\omega_0/W$. For

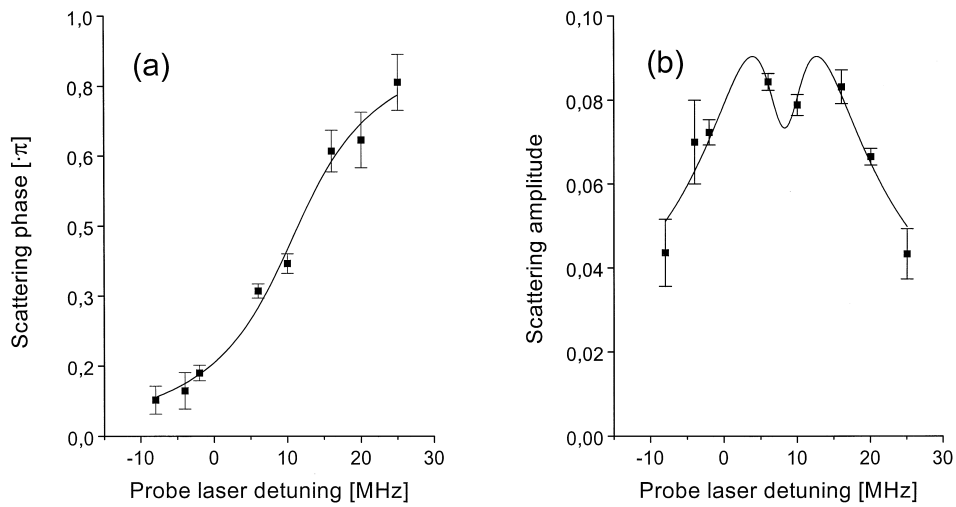

Fig. 3. Spectral dependence of the phase (a) and the amplitude (b) of the scattered Gaussian beam. Solid lines represent fits to a linear oscillator model including saturation by the trapping laser beams.

a linear oscillator model we can replace the index of refraction through Eq. (1) by

$$\arg\Phi_0 = \tan^{-1}\frac{n'-1}{-n''} = \tan^{-1}\frac{2\delta}{\gamma},$$

$$|\Phi_0| = \sqrt{\pi}\,k\,\omega_0\sqrt{(n'-1)^2+n''^2}$$

$$= \frac{3k\omega_0 n_{\mathrm{At}}\lambda^3}{8\pi^{3/2}}\frac{\sqrt{1+(2\delta/\gamma)^2}}{1+s_0+(2\delta/\gamma)^2}, \qquad (9)$$

where in addition saturation was accounted for by the saturation parameter s_0 of the trapping laser beams. The line centers are blue shifted by 10.7 ± 1.2 MHz for the phase and 8.3 ± 1.2 MHz for the amplitude due to the ac Stark effect of the trapping laser. In the fit of the amplitude curve the natural line width γ was fixed to 5.22 MHz and a saturation parameter was fitted to $s_0 = 3.8 \pm 0.4$. This has to be compared to the saturation parameter 6.4 ± 0.4 extracted from the light shift and the one-beam saturation parameter of 4.1 that was determined from the trapping laser intensity. The natural line width of 17.4 ± 1.6 MHz in the phase curve strongly deviates from the theoretical value of 5.22 MHz. This disagreement shows that details of the ligh–matter interaction in the trapped sample are beyond the simple linear oscillator model.

Unusual appearance of the amplitude curve on Fig. 3b is due to the fact that the diffraction pattern depends on the absolute value of the scattering amplitude $|\Phi_0|$ and not on its real (dispersion) or imaginary (absorption) part as in common spectroscopic experiments. According to Eq. (9) a dip in the amplitude curve is predicted for strong saturation $s_0 > 1$.

In a second experiment the frequency dependence of the forward scattering amplitude was investigated with the probe laser frequency scanning across a resonance line. We replaced the screen by a photodiode in the center of the diffraction pattern. An iris diaphragm of 1 mm diameter in front of the photodiode was used to select a central detection area smaller than the width of the central fringe. Here not the spatial but the spectral characteristics of the diffraction can be seen at a glance. Using (8) for $\rho = 0$ and (9), the forward scattering signal reads

$$\frac{|E_{\mathrm{i}}+E_{\mathrm{s}}|^2}{E_0^2} - 1 = -\frac{3}{kz_0}\frac{N}{1+(z/z_0)^2} \times \frac{1+(z/z_0)(2\delta/\gamma)}{1+s_0+(2\delta/\gamma)^2}, \qquad (10)$$

where $N = \pi^{3/2} n_{\mathrm{At}} \omega_0^3$ is the total atom number in the trap.

As expected, due to dispersion on the red and blue side of an atomic resonance the scattered wave is retarded or advanced relative to the incident wave. This explains the appearance of an intensity minimum in the center of the diffraction pattern from the blue detuned probe laser (see

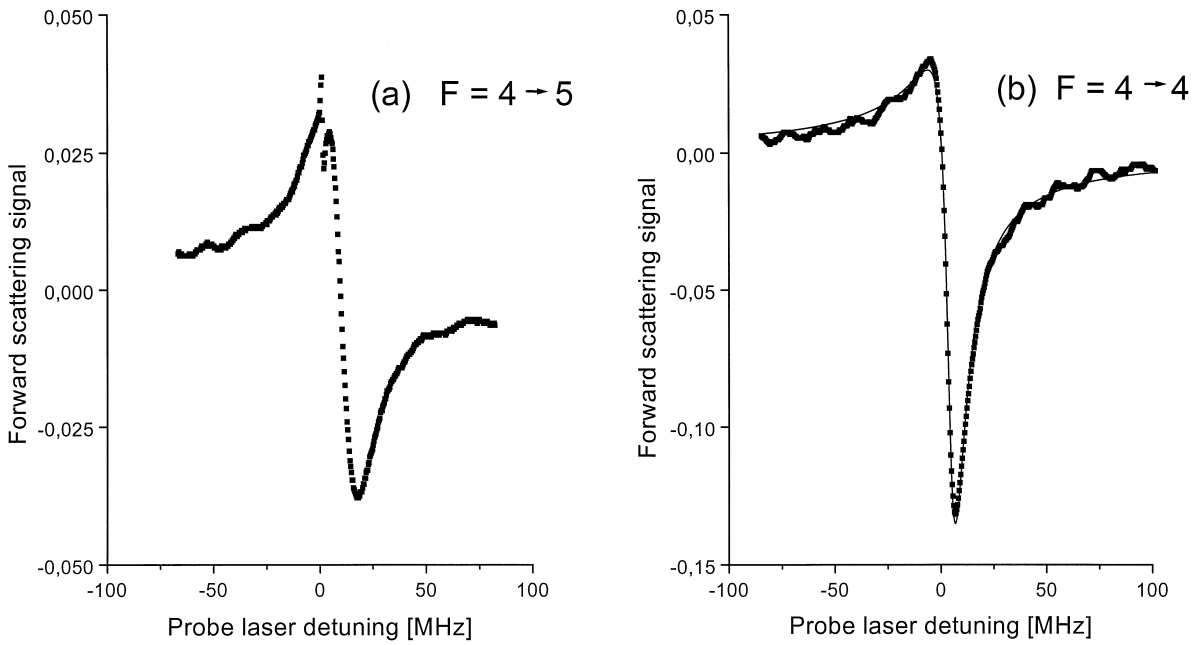

Fig. 4. Forward scattering intensity as a function of probe laser detuning from atomic resonance for the $F = 4 \rightarrow F' = 5$ transition (a) and the $F = 4 \rightarrow F' = 4$ transition (b). Trapping laser intensity is 2.2 mW/cm^2 per laser arm. The solid line in (b) is a fit using Eq. (10). The slight oscillations are due to an etalon effect of the fiber.

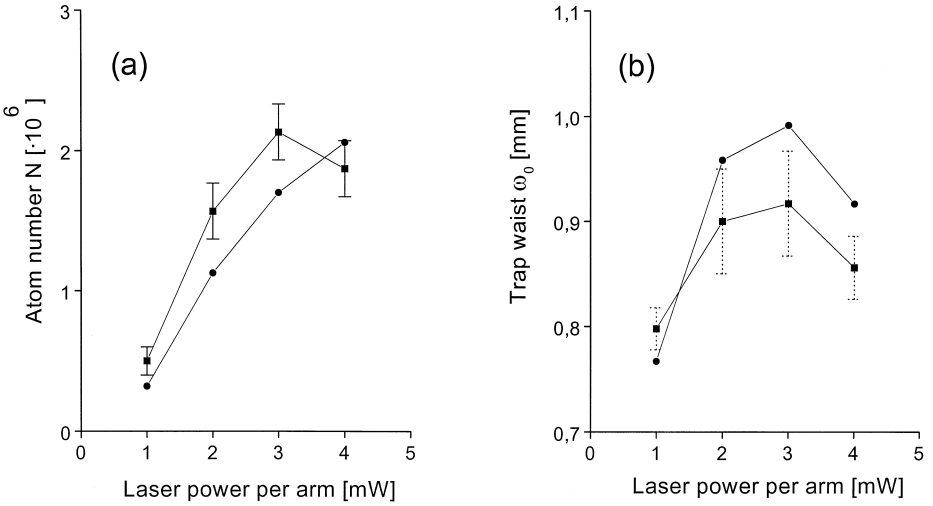

Fig. 5. Comparison of trap parameters measured with forward scattering (squares) and with a calibrated CCD camera (dots): (a) atom number, (b) trap waist. Statistical errors of the values obtained from the fluorescence are small, but the uncertainty in the calibration factor for absolute atom number is of order of 2. The measured waist values are more reliable and have an accuracy better than 10%.

Fig. 4). Note that for very short $z \ll z_0$ an absorption profile (shadow effect) is expected on the screen

$$\frac{|E_i + E_s|^2}{E_0^2} - 1 = -\frac{3N}{kz_0}\frac{1}{1 + s_0 + (2\delta/\gamma)^2}. \qquad (11)$$

At large distance from the MOT $z \gg z_0$ the dispersion part remains relevant only,

$$\frac{|E_i + E_s|^2}{E_0^2} - 1 = -\frac{3N}{kz}\frac{2\delta/\gamma}{1 + s_0 + (2\delta/\gamma)^2}. \qquad (12)$$

In the general case we have a mixture of dispersion and absorption profiles in (10) weighted by the ratio z/z_0, which allows one to obtain information on trap size from the fitting.

First we scanned across the $F = 4 \rightarrow F' = 5$ transition (Fig. 4a), that is the trapping transition at the same time. The power broadened resonance line is seen as a dispersive line. On the red side of this line a sharp extra resonance is recorded when the probe laser frequency coincides with the trapping laser frequency. This resonance has been identified in transmission spectra [2,3,10] as a result of Raman transitions between vibrational levels of atoms localized in optical potential wells. It indicates that nonlinear processes do play a significant role also in the scattering process and hence cause wavefront distortion.

The situation becomes clearer when the $F = 4 \rightarrow F' = 4$ transition is used for probing. In Fig. 4b an example of a forward scattering spectrum is shown together with a fit according to Eq. (10). From the characteristic line form the trap size is extracted. The forward scattering amplitude then gives the atom number.

The same procedure was repeated for different trap laser intensities. In Fig. 5 we present the fitting parameters along with the data from CCD camera pictures that were taken for each scan as a monitor. The deviation is smaller than 10%.

5. Conclusion

We have observed diffraction of a near resonant light field from a trapped sample of cold atoms. The diffraction pattern yields information on the wavefront distortion by cold samples and provides another method for both the determination of the density distribution and the total number of atoms. More precisely, the polarization density may be reconstructed from the holographic records and the relation of atomic dielectric response and wavefront distortion can be studied.

Acknowledgements

This work was supported by the Deutsche Forschungsgemeinschaft. We have much profited from communications with W. Phillips, M. Walhout [13], and U. Sterr of the National Institute of Standards and Technology in Gaithersburg, who pointed out to us the importance of the Fresnel factor in the diffraction pattern. Furthermore we wish to thank R. Wynands for helpful discussions and contributions.

References

[1] E.L. Raab, M. Prentiss, A. Cable, S. Chu, D.E. Pritchard, Phys. Rev. Lett. 59 (1987) 2631.

[2] J.W.R. Tabosa, G. Chen, Z. Hu, R.B. Lee, H.J. Kimble, Phys. Rev. Lett. 66 (1991) 3245.
[3] D. Grison, B. Lounis, C. Salomon, J.-Y. Courtois, G. Grynberg, Europhys. Lett. 15 (1991) 149.
[4] D.W. Sesko, T.G. Walker, C.E. Wieman, J. Opt. Soc. Am. B 8 (1991) 946.
[5] A. Hemmerich, T.W. Hänsch, Phys. Rev. Lett. 70 (1993) 410.
[6] B.J. Thompson, J. Opt. Soc. Am. 53 (1963) 1350; J. Phys. E 7 (1974) 781.
[7] B.W. Peuse, M.G. Prentiss, S. Ezekiel, Phys. Rev. Lett. 49 (1982) 269; Optics Lett. 8 (1983) 154.
[8] M.H. Anderson, J.R. Ensher, M.R. Matthews, C.E. Wieman, E.A. Cornell, Science 269 (1995) 198; K.B. Davis, M.-O. Mewes, M.R. Andrews, N.J. van Druten, D.S. Durfee, D.M. Kurn, W. Ketterle, Phys. Rev. Lett. 75 (1995) 3969; C.C. Bradley, C.A. Sackett, J.J. Tollett, R.G. Hulet, Phys. Rev. Lett. 75 (1995) 1687.
[9] A. Höpe, D. Haubrich, H. Schadwinkel, F. Strauch, D. Meschede, Europhys. Lett. 28 (1994) 7.
[10] P. Verkerk, B. Lounis, C. Salomon, C. Cohen-Tannoudji, Phys. Rev. Lett. 68 (1992) 3861.
[11] A. Hemmerich, M. Weidemüller, T. Esslinger, T. Hänsch, Europhys. Lett. 21 (1993) 445.
[12] M. Abramowitz, I.A. Stegun, Handbook of Mathematical Functions (Dover, New York, 1970).
[13] M.S. Walhout, Studies of Laser-Cooled and Magneto-Optically Trapped Xenon, Ph.D. Thesis, University of Maryland (1994).